行政院國家科學委員會專題研究計畫　成果報告

總計畫

計畫類別：整合型計畫
計畫編號：NSC91-2120-E-002-003-
執行期間：91 年 08 月 01 日至 92 年 10 月 31 日
執行單位：國立臺灣大學電子工程學研究所

計畫主持人：林浩雄
共同主持人：毛明華，白偉武

報告類型：完整報告

處理方式：本計畫可公開查詢

中　華　民　國 92 年 11 月 13 日

行政院國家科學委員會專題研究計畫成果報告

前瞻性量子元件技術

計畫編號: NSC-91-2120-E-002-003

執行期限:91/08/01~92/07/31

主持人:林浩雄　共同主持人：白偉武、毛明華

執行單位:國立台灣大學

摘要

本計畫包括以固態源分子束磊晶機在砷化鎵基板上成長銻砷化鎵/砷化鎵第二型量子井雷射二極體、砷化銦/砷化銦鎵量子點、以橫截面掃描式穿隧顯微鏡(XSTM)研究砷化銦量子點成長機制以及量子點雷射等研究。在第二型量子井的部分我們達到波長1300nm、半寬80meV的室溫光激螢光譜。單量子井雷射的室溫振盪波長達1290nm，起振電流密度達300A/cm^2。在XSTM的部分，我們在InAs量子點上以三種方法(SMD、SMEE及MBE)成長$In_{0.33}Ga_{0.67}As$覆蓋層，並以統計方法分析此三種量子點橫截面應力分佈，我們推論出以SMD方法成長覆蓋層的量子點擁有較長波的激發光譜，是因為其量子點有較弱的量子侷限作用。相反的，以SMEE方法成長覆蓋層的量子點擁有較短波的激發光譜，乃在於其量子點有較強量子侷限作用以及量子點內部銦的含量較少。我們提出合理的可能成長機制，並對成長長波長量子點樣品提供改進的方向。在元件方面，我們成功地製作出室溫發光波長在1295 nm的砷化銦/砷化銦鎵量子點雷射。所測得最高的鬆弛震盪頻率為1.8 GHz，對應的調變頻寬達2.8 GHz。

關鍵詞: 分子束磊晶，含銻化合物半導體，銻砷化鎵量子井，砷化銦量子點，橫截面掃描式穿隧顯微鏡，量子點雷射，鬆弛震盪。

Abstract

The studies of this project include the molecular beam epitaxial (MBE) growth of GaAsSb type-II quantum well (QW) and InAs/InGaAs quantum dot (QD), cross-section scanning tunneling microscopy (XSTM) technique for QD, and the related long wavelength laser diodes. In the first portion, GaAsSb/GaAs type-II QW and its laser device were grown. The PL emission wavelength of the QW successfully reaches 1300m with a FWHM of 80 meV. On the results of the type II GaAsSb/GaAs single quantum well laser diode on GaAs substrate, a low threshold current density of 300A/cm^2 and an emission wavelength of 1290nm are demonstrated at room temperature. In the second portion, we use XSTM to examine strain relaxation profile of the ensembles of InAs QDs with overgrown $In_{0.33}Ga_{0.67}As$ layers prepared by three distinct methods, i.e. SMD, SMEE, and MBE. A statistical analysis of strain relaxation profile allows us to infer that longest wavelength of SMD sample is due to weaker confinement, and the shortest wavelength of SMEE sample is due to both larger confinement and lower In ratio in QDs. We rationalize plausible growth mechanisms and suggest routes for further improvement. Finally, InAs/InGaAs quantum-dot lasers with emission wavelength at 1295 nm at room temperature are fabricated. The highest relaxation oscillation frequency measured at room temperature is 1.8 GHz, corresponding to a modulation bandwidth of 2.8 GHz.

Keywords: molecular beam epitaxy, Sb-based compound semiconductor, GaAsSb quantum well, InAs quantum dot, cross-section STM. quantum-dot laser, relaxation oscillation.

Introduction

GaAsSb/GaAs type-II semiconductor heterostructure has drawn a lot of interest in recent years due to its capability of emitting photons with energy less than fundamental band gaps of each layer, and is an important candidate for low cost 1300nm light source. Recently we have successfully grown a low threshold current GaAsSb/GaAs double quantum well (QW) laser that emits at 1280 nm [1]. For the design of GaAsSb/GaAs type-II devices, the band alignment is an essential parameter. However, the earlier studies on the band lineup between GaAs and GaAsSb gave scattered results. In terms of valence band offset ratio $Q_v = \Delta E_v/\Delta E_g$, the reported data ranges from 1.05 to 2.1 [2-3]. Most of these studies used photoluminescence (PL) to determine the transition energy of the QW with different well width. However, the band bending induced by spatially separated electrons and holes may cause significant blue shift on the PL peak wavelength as excitation level increases, [3-4] and makes the determination of flat band transition energy rather difficult. We propose a simple method to derive the flat-band transition energies in these type-II QWs. And by fitting the transition energy versus the quantum well width, the GaAsSb/GaAs valence band offset ratio can be derived.

Since proposed in 1982 [5], quantum-dot (QD)

lasers have attracted much attention due to their superior properties compared with quantum-well lasers [6]. Recently, there was much interest in 1.3 μm In(Ga)As quantum-dot lasers [7-9], because they show very low threshold current density and they serve as a candidate for light sources in fiber communication systems. However, the fabrication and applications of InGaAs based quantum dot (QD) lasers operating at 1300 or 1550nm [10-15] involve challenging issues in materials preparation. This is mainly due to the difficulty in achieving simultaneously smaller band gap and larger size of defect-free InGaAs quantum dots. There are two routes to achieve long wavelength (>1300nm) light emission from InAs quantum dots. They are (1) sub-monolayer migration enhanced deposition of $In_xGa_{1-x}As$ quantum dots (x~0.5) [16], and (2) InGaAs layers bordering quantum dots on one or both sides[14,17]. The growth kinetics of capping layer affects QDs and their emission wavelength. We perform a XSTM study to examine the strain relaxation profiles of buried QDs. We develop an analysis approach to characterize the relationship between outward relaxation volume, base width, and height on the QD ensemble. This provides sufficient statistics and allows us to infer trends of In concentration variation and dot shape change under different capping methods. Based on the result of XSTM results, InAs/InGaAs quantum-dot lasers with emission wavelength at 1295 nm are fabricated and their dynamic properties will be investigated through the measurement of relaxation oscillations (RO). Concerning the dynamic properties of QD lasers, there were several studies in the literature [18-21]. But only very few of them are for QD lasers in 1.3 μm wavelength range [21].

Results and Discussions

In the study of GaAsSb/GaAs quantum well, we used VG V80MKII solid source molecular beam epitaxy to grow the heterostructure. As_4 and Sb_1 sources were from a Riber VAC500 valve cracker and an EPI 175 Sb cracker, respectively. The growth temperature of GaAsSb/GaAs quantum well was 500°C, and the growth rate was ~ 1μm/hr. The active medium of the laser is a 7-nm-thick GaAsSb quantum well with 80-nm-thick GaAs barrier. $Al_{0.6}Ga_{0.4}As$ was used as the cladding layers and the growth temperature was 580°C. The active layer was enclosed within an undoped separate confinement heterostructure (SCH) composed of two 100-nm-thick AlGaAs graded index (GRIN) layers. By increasing Sb content in the GaAsSb well, the PL emission wavelength can be extended to 1300 nm. Fig. 1 shows the PL spectrum of the GaAsSb/GaAs single quantum well laser after the top p-cladding layer being removed. The peak position is at 1300 nm, and the FWHM is about 80 meV. 50-μm-wide broad stripe lasers with different cavity lengths were fabricated. Fig. 2 displays the L-I characteristic of the grown laser under pulsed mode operation. The threshold current density is ~300 A/cm^2. Fig. 3 shows the spectrum of a laser with a cavity length of 2.2 mm. The lasing wavelength is 1292 nm.

The GaAsSb/GaAs QW samples used for the band alignment determination were grown by solid source molecular beam epitaxy. The growth parameters are the same as described above except the As source was from a conventional thermal K-cell. Type-II $GaAs_{0.7}Sb_{0.3}$/GaAs single and multiple QWs with different well thickness ranging from 3 nm to 9 nm were grown. All type-II QW samples are capped with 100-nm-thick GaAs. The compositions of the layers were determined from a Bede QC200 high resolution X-ray diffractometer. Photoluminescence spectroscopy (PL) was used to measure the transition energies of the QWs. Fig. 4 shows the excitation power dependence on the PL peak energy shift of a $GaAs_{0.7}Sb_{0.3}$/GaAs MQW. As can be seen, the QW exhibits a very significant blue shift as the excitation power is increased. In order to extract the flat-band transition energy of the type-II GaAsSb/GaAs QW, we derived a simple one-third root relation between the electron quantization energy and the integrated PL intensity [22-23]. Fig. 5 shows the PL peak energy as a function of the third root of the integrated intensity in the power dependent PL measurement of a GaAsSb/GaAs QW. As can be seen, the PL peak energy follows the expected behavior. The intercept of the plot corresponding to zero integrated intensity, which implies zero electric field, is the flat-band transition energy of the type-II QW. Fig. 6 shows the flat-band energy of $GaAs_{0.7}Sb_{0.3}$ as a function of QW width. The valence band offset ratio Q_v can be derived from the flat-band transition energy of QWs with different well width. The band gap energy of the $GaAs_{0.7}Sb_{0.3}$ and the strain induced shift on its heavy-hole band gap were calculated. By using Q_v as the fitting parameter, the flat-band transition energies of different well widths were then calculated to fit the experiment data. The fitted Q_v of $GaAs_{0.7}Sb_{0.3}$/GaAs heterostructure is 1.32.

In the XSTM study of the InAs/InGaAs QD, the structure of the sample is shown in Fig. 7. It consists of SMEE, SMD, and MBE layers grown on Te doped GaAs(100) wafer with identical conditions except the III-V element deposition sequence. The InGaAs layer is overgrown on top of InAs QDs with alternating gated column III element fluxes. Three methods are tested and their respective growth sequence of In, Ga, As fluxes are depicted in Fig. 8. It is found that emission wavelength λ(SMD)>λ(MBE) >λ(SMEE) as shown in Fig. 9.

We resort to a less quantitative approach in which the outward strain relaxation profile of each QD is analyzed. Figure 10(b) and 10(c) show line profiles in the growth direction and along the QD layer. It is noted that the tail of the strain relaxation profile (fig. 10b) is dominated by the $In_{0.33}Ga_{0.67}As$ overgrown layer. From contact mechanics [24] one can deduce the strain relaxation profile as

$$z = C - \frac{2(1+\upsilon)\varepsilon_0}{\pi} \times \left[(x+a)\log\left|\frac{x+a}{a}\right| - (x-a)\log\left|\frac{x-a}{a}\right| \right]$$

,where C is a baseline constant, υ is Poisson ratio, ε_0 is strain, and a is half QW width. We estimate the width of the $In_{0.33}Ga_{0.67}As$ layer directly from STM images and found it to be ~5nm in all SMEE, MBE, SMD layers. This is larger than the expected 2.6nm, indicating significant intermixing occurs during GaAs spacer growth. We approximate the 2.6nm thick $In_{0.33}Ga_{0.67}As$ layer with a 5nm thick $In_{0.17}Ga_{0.83}As$ layer (to keep total In constant) and fit the outward relaxation profile to the experimental data. This is shown as the red line in Fig. 11. Subtracting this profile, we obtained more accurate strain relaxation profile of a QD as the green line shown in Fig. 11. This profile is further fitted by a Lorentz function. Fitted heights (z) are plotted along the QD layer similar to the one shown in Fig. 10(c). The base width (w) of each QD is directly obtained from such a plot and the QD height (h) is taken as the Lorentz FWHM at the base center. Finally, the outward volume (V) is obtained by integration of $dz*dw*dh$.

Figure 12 shows a step-free cross-sectional view of the three studied QD layers (shown with arrows in Fig. 7). Closer inspection reveals that MBE capped QD appears more uniform in its In distribution. In both the SMD and SMEE samples, variation of contrast in the QDs and capped layer often appears and is most evident for the SMEE sample. Such a contrast variation can be related to spatial variation of In. Thus, alloy decomposition in SMD and SMEE samples is significant.

Typical STM images of the SMEE, SMD, MBE QDs are shown in Fig. 13(a)-(c). We have analyzed a total length of ~10 μm along the QD layer for each growth method, with their outward relaxation volume, base width, and dot height obtained from the above outline procedure. Table II lists the average V, w, h values and the QD densities.

The trend of average dot height is consistent with the photoluminescence (PL) result. SME QDs has the smallest $<h>$ and SMD QDs has the largest $<h>$. The QD shape is also different. SME QDs are shallowest with an aspect ratio ~1/6, as compared with the ~1/4 ratio of MBE and SMD QDs. Because the PL wavelength depends on both band gap value and quantum confinement effect, we also evaluate statistical average of In concentration in the QDs. We evaluate its trend by plotting the outward volume V vs. dot base width w * dot height h. The dependence of V on w and h should lie between $w*h$ and at most w^2*h. In the former case, it assumes the strain relaxation comes from the surface layer and the latter assumes the strain relaxation from embedded volume has weak z dependence. Reality should lie in between. We have plotted V vs. wh and V vs. w^2h, and we performed a linear fit passing the origin. In both cases, we found the slope s has similar trend in which s(MBE) > s(SMD) > s(SME). Therefore, for a fixed value of $w*h$, the outward volume is largest for MBE QD, implicating the average In concentration in MBE QDs is slightly larger. A V vs. $w*h$ plot is shown in Fig. 14.

Different preparation methods of capping layers influence the optoelectronic performance of quantum dots. This is mainly a consequence of growth kinetics. Our analysis strongly indicates that capping with Ga migration enhanced deposition should be avoided. This is directly related to easier Ga incorporation in absence of As flux. [25] The low In concentrations of SMEE dots lead to large QD sizes. Yet this larger QD size is not particularly helpful as three concomitant detrimental effects occur, namely decrease of dot height and dot aspect ratio, reduction of In concentration, and reduction of dot density. In the SMD method, it has been suggested [26] that Ga atoms prefer to migrate away from the InAs quantum dot during GaAs deposition to match the lattice constant of unstrained GaAs (i.e. strained InAs wetting layer). From the PL results, it appears that the weaker quantum confinement effect has overtaken the smaller band gap in MBE QDs, resulting in the longest wavelength of SMD dots. One possible improvement of QDs for long wavelength light emission is suggested. In preparation of the InGaAs capped layer, one may use alternating submonolayer deposition of firstly the SMEE-grown InAs and then SMD-grown GaAs. Optimization of such a capping layer growth would be fine-tuning growth parameters instead of growth sequence.

The sample designed for 1.3μm QD lasers is grown using gas-source molecular beam epitaxy (GSMBE) on Si-doped n+ (100) GaAs substrate. In the center of the waveguide, there are three stacks of QD layers. For each QD layer, 2.3 monolayer (ML) InAs was firstly deposited and followed by a 9.0 ML $In_{0.33}Ga_{0.67}As$ capping layer. These three stacks of QD layers are then embedded in a 200-nm-thick waveguide layer with $In_{0.49}Ga_{0.51}P$ serving as upper and lower cladding. A heavily p^+-doped ($1.5\times10^{19}cm^{-3}$) 200-nm-thick GaAs layer is grown as contact layer. After the epitaxial growth, the wafers were processed into 8-μm-wide ridge waveguide lasers with different cavity lengths by using standard photolithography, wet etching, and metallization techniques. The fabricated lasers were tested under pulsed mode with a pulse width 500 ns and a repetition rate of 5 kHz to measure the static properties. In Fig. 15, ground-state lasing at 1295 nm at room temperature with nominal threshold current density of 152.5 A/cm^2 is demonstrated from a laser structure of 3.5 mm long and 8 μm wide. With this low threshold current (I_{th}= 42.7 mA), it is possible to investigate the relaxation oscillations.

For the dynamic measurement, we use an ultra-high speed pulse generator, a photo detector, a pre-amplifier, and a 50GHz oscilloscope to observe the relaxation oscillations. Fig. 16 shows a linear dependence of RO frequencies on the square root of normalized current, as predicted theoretically [27]. The highest relaxation oscillation frequency measured

is 1.8 GHz, corresponding to a modulation bandwidth of 2.8 GHz [28].

Conclusion

We have extended the lasing wavelength of the GaAsSb/GaAs quantum well laser to 1290 nm successfully. The threshold current density is 300A/cm^2. The GaAsSb/GaAs band alignment was also studied by measuring the PL of the $GaAs_{0.7}Sb_{0.3}$/GaAs quantum wells. By proposing a simple method to exclude the band bending induced blue shift in power dependent photoluminescence, we derived the valence band offset ratio Q_v of GaAsSb/GaAs QW. The result is 1.32.

In the XSTM study of the InAs/InGaAs QDs, strain relaxation profile of ensembles of InAs QDs with overgrown $In_{0.33}Ga_{0.67}As$ layers prepared by three distinct methods, i.e. SMD, SMEE, and MBE, has been studied. A statistical analysis of strain relaxation profile allows us to derive their outward relaxation volume, base width, and dot height. The longest wavelength of SMD sample is due to weaker confinement, and the shortest wavelength of SMEE sample is due to both larger confinement and lowers In ratio in QDs. InAs/InGaAs quantum-dot lasers with emission wavelength at 1295 nm at room temperature are also fabricated. The highest relaxation oscillation frequency measured at room temperature is 1.8 GHz, corresponding to a modulation bandwidth of 2.8 GHz. For 1.3 μm QD lasers, this is one of the best values in the literature. Thus, the application potential of long-wavelength QD lasers for fiber communication is demonstrated.

References:

1. P. W. Liu, M. H. Lee, H. H. Lin, and J. R. Chen, Electron. Lett. **38**, 1354 (2002).
2. M. Peter, K. Winkler, M. Maier, H. Herres, J. Wagner, D. Fekete, K. H. Bachem, and D. Richards, Appl. Phys. Lett. **67**, 2639 (1995).
3. R. Teissier, D. Sicault, J. C. Harmand, G. Ungaro, G. Le Roux, and L. Largeau, J. Appl. Phys. **89**, 5473 (2001).
4. D. Vignaud, X. Wallart, F. Mollot, and B. Sermage, J. Appl. Phys. **84**, 2138 (1998).
5. Y. Arakawa, and H. Sakaki, Appl. Phys. Lett., **40**, 393 (1982).
6. D. Bimberg, M. Grundmann, and N. N. Ledentsov, *Quantum Dot Heterostructures*, Wiley, 1999.
7. Zhukov, A. E., A. R. Kovsh, V. M. Ustinov, Yu. M. Shernyakov, S. S. Mikhrin, N. A. Maleev, E. Yu. Kondrat'eva, D. A. Livshits, M. V. Maximov, B. V. Volovik, D. A. Bedarev, Yu. G. Musikhin, N. N. Ledentsov, P. S. Kop'ev, Zh. I. Alferov, and D. Bimberg, IEEE Phot. Tech. Lett. **11**, 1345 (1999).
8. D. L. Huffaker, G. Park, Z. Zou, O. B. Shchekin, and D. G. Deppe, "1.3 μ m room-temperature GaAs-based quantum dot laser," Appl. Phys. Lett., **73**, 2564 (1998).
9. Liu, G. T., A. Stintz, H. Li, K. J. Malloy, and L. F. Lester. Electron. Lett., **35**, 1163 (1999).
10. K. Nishi, H. Saito, S. Sugou, and J. S. Lee, Appl. Phys. Lett. **74**, 1111 (1999).
11. G. Park, O. B. Shchekin, S. Csutak, D. L. Huffaker, and D. G. Deppe, Appl. Phys. Lett. **75**, 3267 (1999).
12. G. Park, D. L. Huffaker, Z. Zou, O. B. Shchekin, and D. G. Deppe, IEEE Photonics Technol.Lett. **11**, 301 (1999).
13. G. Park, O. B. Shchekin, D. L. Huffaker, and D. G. Deppe, IEEE Photonics Technol. Lett. **12**, 230 (2000).
14. A. Stintz, G. T. Liu, H. Li, L. F. Lester, and K. J. Malloy, IEEE Photonics Technol. Lett. **12**, 591 (2000).
15. V. M. Ustinov, A. E. Zhukov, A. R. Kovsh *et al.*, Microelectron. J. **31**, 1 (2000).
16. D. L. Huffaker *et al.*, Appl. Phys. Lett. **73**, 2564(1998).
17. V. M. Ustinov, N. A. Maleev, A. E. Zhukov *et al.*, Appl. Phys. Lett. **74**, 2815 (1999).
18. M.-H. Mao, F. Heinrichsdorff, A. Krost and D. Bimberg, Electron. Lett., **33**, 1641 (1997).
19. Kamath, K., Phillips, J., Jiang, H., Singh, J., and Bhattacharya, P. Appl. Phys. Lett. **70**, 2952, (1997).
20. P. Bhattacharya, and S. Ghosh, Appl. Phys. Lett. **80**, pp. 3482, 2002.
21. Kuntz, M.; Ledentsov, N. N.; Bimberg, D.; Kovsh, A. R.; Ustinov, V. M.; Zhukov, A. E.; Shernyakov, Yu. M. Appl. Phys. Lett., **81**, pp. 3846, 2002.
22. C. Weisbuch, B. Vinter, Quantum Semiconductor Structures (Academic, Boston, 1991), p.20.
23. N. N. Ledentsov, J. Böhrer, M. Beer, F. Heinrichsdorff, M. Grundmann, D. Bimberg, S. V. Ivanov, B. Ya. Meltser, S. V. Shaposhnikov, I. N. Yassievich, N. N. Faleev, P. S. Kop'ev, and Zh. I. Alferov, Phys. Rev. B **52**, 14058 (1995).
24. K. L. Johnson, Contact mechanics (Cambridge UP, Cambridge, 1985), Sec. 2.5.
25. H. Yamaguchi and Y. Horikoshi, J. Appl. Phys. **68**, 1610 (1990).
26. J. Gebauer, E. R. Weber, N. D. Jäger, K. Urban, and Ph. Ebert, Appl. Phys. Lett. **82**, 2059 (2003).
27. Lau, K.Y., and Yariv, A. IEEE J. Quantum Electron. **QE-21**, 121 (1985).
28. M.-H. Mao, T.-Y. Wu, F.-Y. Chang, and H.-H. Lin, 2003 IEEE LEOS Annual Meeting, Tucson, Oct. 2003.

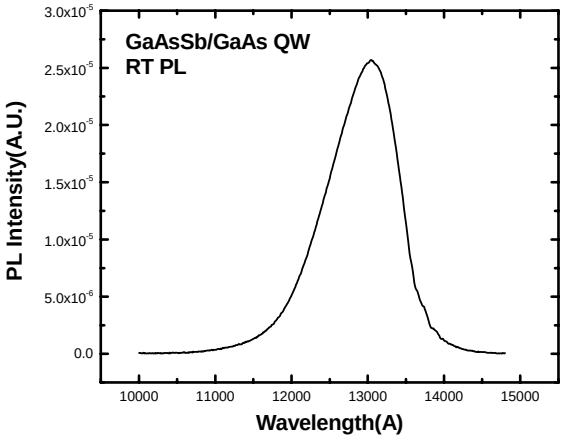

Fig. 1 Room temperature PL spectrum of the grown GaAsSb/GaAs single quantum well laser. The top p-cladding has been removed.

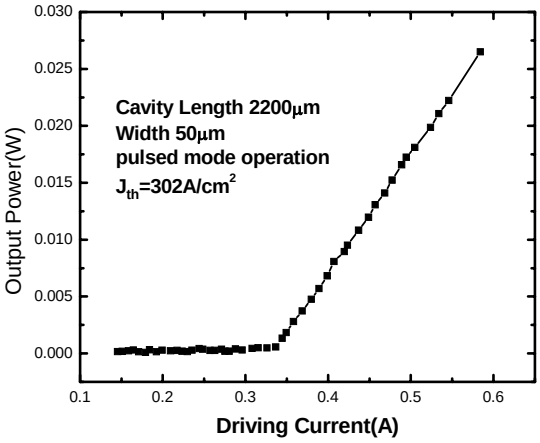

Fig. 2 Light output versus injection current characteristics of GaAsSb/GaAs SQW laser.

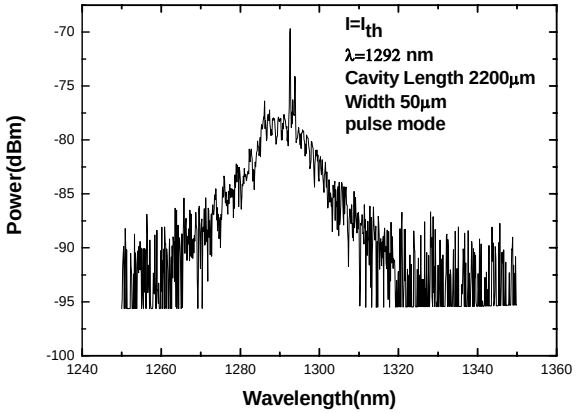

Fig. 3 Lasing spectrum of GaAsSb/GaAs SQW laser.

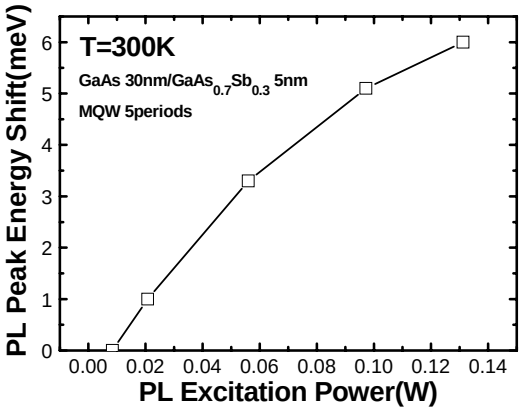

Fig. 4 Excitation power dependence of a $GaAs_{0.7}Sb_{0.3}$/ GaAs QW PL peak energy.

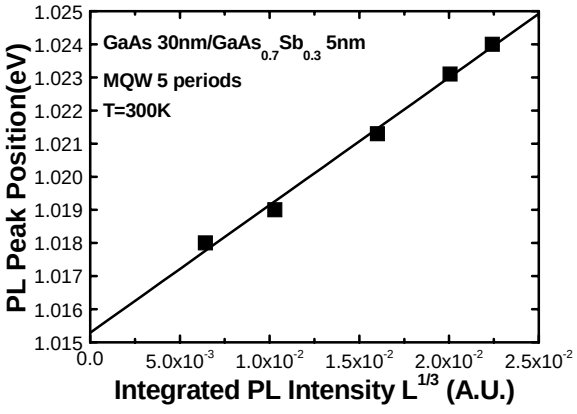

Fig. 5 $GaAs_{0.7}Sb_{0.3}$/GaAs QW PL peak position as a function of the cubic root of the integrated PL intensity.

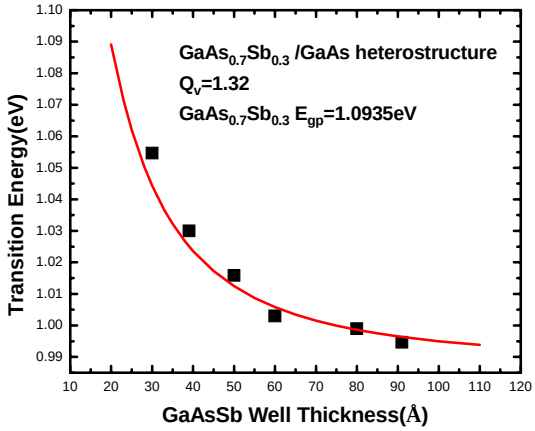

Fig. 6 PL transition energy versus well thickness plot of $GaAs_{0.7}Sb_{0.3}$/GaAs heterostructures. The fitted Q_v is 1.32.

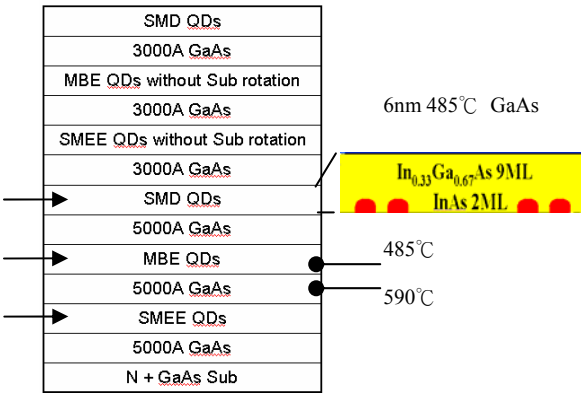

Fig. 7 Schematics of sample structure. Flux of III-V elements and temperature used in each QD layer is shown on the right.

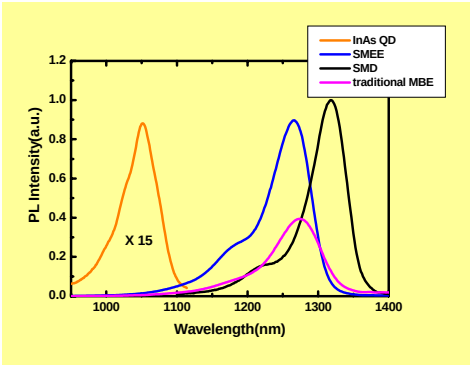

Fig. 9 Photoluminesence (PL) spectrum of InAs/ InGaAs QD. For all MBE, SMEE, SMD grown samples, growth temperature and flux are the same except the different growth sequences.

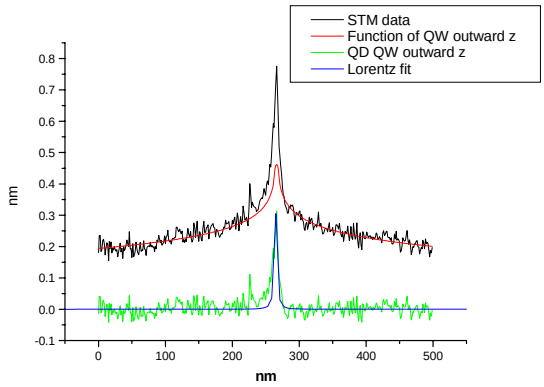

Fig. 11 A line profile normal the QD layer. The red line is the strain relaxation profile of a 5nm $In_{0.17}Ga_{0.83}As$ quantum well with the center position as a fitting parameter. The green line is the residual strain relaxation due to QD. Vertical outward buckle z and QD height h are deduced from a Lorentz fit.

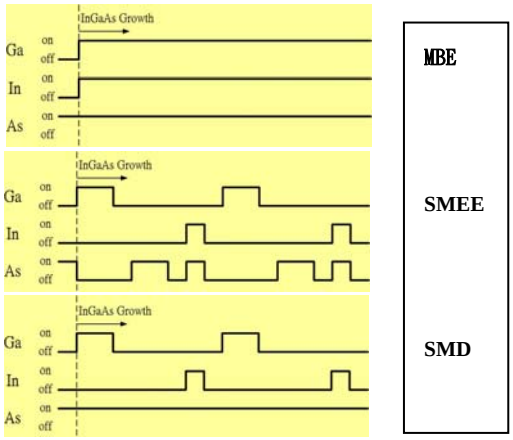

Fig. 8 Schematics of deposition sequences in MBE, SMEE (surface migration enhanced epitaxy), and SMD (submonolayer deposition) methods.

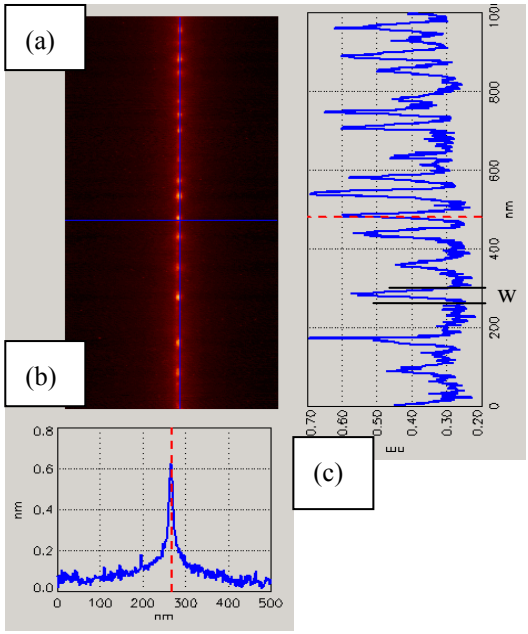

Fig. 10 (a) XSTM view of a QD layer. (b) A line profile normal to the QD layer. (c) A line profile parallel to the QD layer

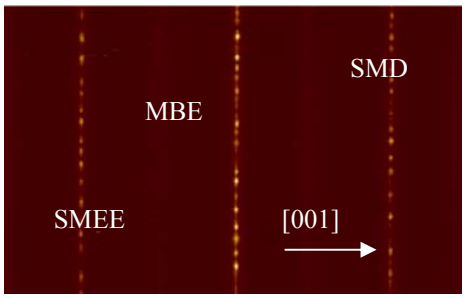

Fig. 12 XSTM image of the SMEE, MBE, SMD layers. Image size=1.5 μm x 1.0 μm, V_s=+2.3V, I_t=0.1nA.

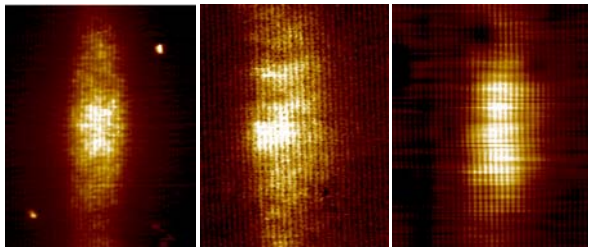

Fig. 13 Typical XSTM images of (a) SMEE (b) SMD (c) MBE capped InAs QDs.

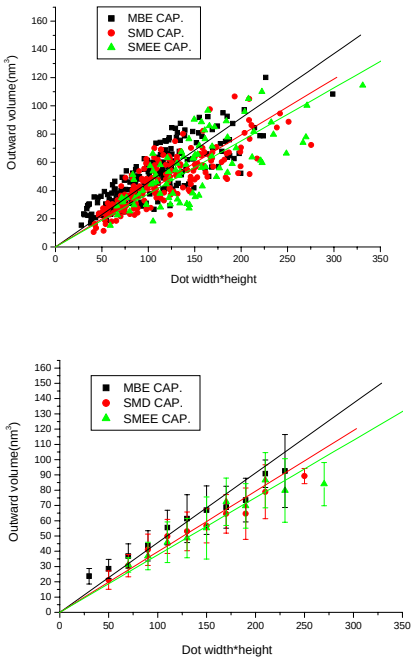

Fig. 14 Plots of outward volume (V) vs. $w * h$ (w: QD base width and h: QD height). Upper panel: raw data. Lower panel: dot width*dot height averaged plot ($w*h$ binsize = 20nm^2).

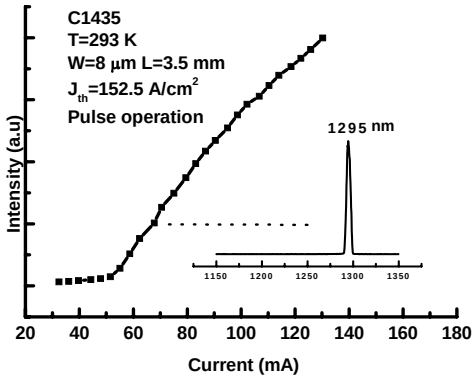

Fig. 15. L-I curve of a QD laser with emission wavelength at 1295 nm.

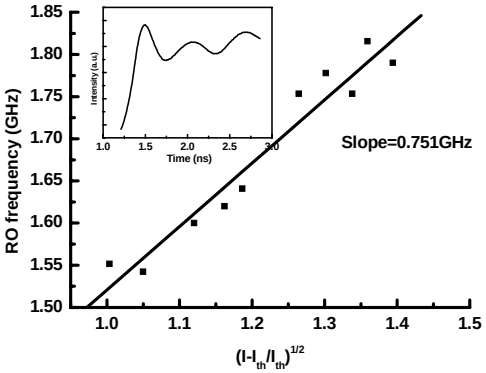

Fig. 16. Relaxation oscillation frequencies v.s. square root of normalized current. The highest RO frequency is about 1.8 GHz.